EPJ E
Soft Matter and Biological Physics
EPJ.org
your physics journal

Eur. Phys. J. E (2020) **43**: 18 DOI 10.1140/epje/i2020-11942-3

Activity-modulated phase transition in a two-dimensional mixture of active and passive colloids

Mohammed Elismaili, Samah Hamze, Hong Xu and David Gonzalez-Rodriguez

edp sciences Società Italiana di Fisica Springer

Eur. Phys. J. E (2020) **43**: 18
DOI 10.1140/epje/i2020-11942-3

THE EUROPEAN PHYSICAL JOURNAL E

Regular Article

Activity-modulated phase transition in a two-dimensional mixture of active and passive colloids*

Mohammed Elismaili, Samah Hamze[a], Hong Xu[b], and David Gonzalez-Rodriguez[c]

Université de Lorraine, LCP-A2MC, F-57000 Metz, France

Received 14 October 2019 and Received in final form 18 February 2020
Published online: 9 March 2020

Abstract. We study a two-dimensional binary mixture of active and passive colloids as an idealized model of an hybrid aggregate of living cells and inert particles. We perform molecular dynamics simulations of this system using two different thermostats, and we systematically investigate the effect of varying these two effective temperatures on the system behavior, as characterized by its density, structure and thermoelastic properties. Our results indicate that the presence of active colloids shifts the mixture towards the liquid state and renders it more deformable. Such system softening and melting effects due to the addition of active particles are larger than expected from a linear combination of temperatures of the active and passive components. This heightened effect becomes more pronounced as the effective temperature difference between the two components becomes larger. The binary mixture remains homogeneous for moderate colloidal activity, but segregation arises for large effective temperature difference. Our results provide insights to guide future experimental hybrid aggregate studies with promising biomedical applications.

1 Introduction

Active colloids, a type of active matter, are particles that harvest energy from their environment or from an internal reservoir and transfer it to their surroundings, thus keeping the system out of equilibrium [1]. This energy flux fuels colloidal activities such as self-motility. The most widely studied type of active colloids are particles with active directional propulsion, where the swimming direction is randomized by rotational diffusion (the so-called Active Brownian Particles) or by tumbling events (Run-and-Tumble Particles) [2]. These models were originally developed to represent bacterial swimming, and they can also be applied to other realms of active matter, such as molecular motors [3] or synthetic Janus colloids [4]. A less studied type of active colloids are those whose self-motility is enhanced diffusion rather than directional propulsion, such as vibrated granular media [5] and chromatine [6]. The two types of active motility, directional or non-directional, have respectively been termed as "vectorial" or "scalar" activity [7]. In this article we study scalar active colloids. This choice is motivated by the study of non-directional motion of cells in a tissue, which can in certain cases be described as a zero-mean Brownian motion [8,9], and which has been modeled as non-directional active motion in earlier computer simulations [10–13].

Important insights into the physics of tissues have been provided by cellular aggregates, a laboratory model to study developing tissues and tumors [14] and an example of so-called entangled active matter [15]. Recent experimental work has investigated hybrid cellular aggregates, formed by a mixture of inert particles and active cells [16,17]. These studies have opened new prospects for nanoparticle-based cancer therapies, where particles could modify the tumor's material properties by increasing its cohesivity and reducing its deformability, thus constraining tumor spreading. Crucial to this application is to understand how the material properties of a hybrid aggregate are modulated by its composition, and whether particles and cells can mix rather than segregate. These questions lead us to investigate the fundamental physics of phase transition, order, and thermomechanical properties of a mixture of active and passive colloids.

In this paper, we consider an idealized two-dimensional mixture of scalar active and passive colloids of identical size and interacting through Lennard-Jones potentials, which we investigate by molecular dynamics simulations. To model colloidal activity, we use the concept of an *effective temperature* [7,18], which describes the energy harvesting by active colloids and its dissipation to

* Supplementary material in the form of a .pdf file available from the Journal web page at
https://doi.org/10.1140/epje/i2020-11942-3

[a] *Present address*: LGCGM, EA3913, Université de Rennes, Rennes, France.
[b] e-mail: hong.xu@univ-lorraine.fr
[c] e-mail: david.gr@univ-lorraine.fr

produce non-directional motion. The definition of an effective temperature in vectorial active colloids has spurred much controversy, leading to the conclusion that this concept can only be consistently defined in specific systems [2, 19]. Defining an effective temperature in scalar active colloids, as studied here, is simpler, as this effective temperature can be simply regarded as an enhanced diffusivity of the active component [20,21].

Here we study the role of activity in the solid-liquid phase transition, in the thermomechanical properties of the mixture, and in the emergence of segregation between active and passive components. Characterizing the solid-liquid transition is important to understand how the introduction of inert particles can rigidify a cellular aggregate. Previous studies investigated crystallization of a single-component suspension of self-propelled particles [22] or of self-propelled hard disks [23,24], as well as the role of activity in promoting crystallization in a mixture of active and passive hard spheres [25,26]. Here we focus on studying how colloidal activity modifies the average temperature at melting. Moreover, we characterize the dependence of the system's thermomechanical properties, *i.e.* the shear modulus and the bulk modulus, on the effective temperature of the components. We also investigate segregation induced by differential activity. Activity-induced segregation has been extensively studied for vectorial active matter, either by directly including a self-propulsion term in the equations of motion [19,27,28] or by deriving an effective many-body interaction potential [29]. Segregation in scalar active matter has received comparatively less attention so far, although segregation mechanisms have also been identified. These are based on activity-induced short-range [7,20] and long-range [21] particle attraction.

In the following, we first describe our model and simulation technique. Then we present our results on solid-liquid phase transition, thermomechanical properties, and segregation between the active and passive components. We conclude by summarizing our main findings and highlighting their biophysical implications.

2 Model and simulation technique

2.1 Model

We study a two-dimensional Lennard-Jones binary mixture, representing an active and a passive species. In the absence of directional motility, as considered here, a biologically active species is characterized by shape fluctuations leading to enhanced non-directional motion. We model such activity by defining two different *effective temperatures*, $T_1 > T_2$. The temperature difference is denoted by $\Delta T = T_1 - T_2$. The effective temperature of species i, T_i, is related to its measurable kinetic energy, $E_{\mathrm{k},i}$, by $\langle E_{\mathrm{k},i} \rangle = k_{\mathrm{B}} T_i$, where the angle brackets denote statistical average, k_{B} is the Boltzmann constant and $i = 1, 2$. Temperature uniformity is prevented by a continuous input of energy, which in the biological system is provided by the metabolic activity. We model this energy flux by considering that our two species are in contact with two different thermostats.

We perform molecular dynamics simulations on a system consisting of $N = 1250$ particles interacting through a shifted and truncated Lennard-Jones potential:

$$\phi_{ij}(r) = \begin{cases} 4\epsilon_{ij}\left[\left(\frac{\sigma}{r}\right)^{12} - \left(\frac{\sigma}{r}\right)^{6}\right] - u_0, & \text{if } r \le r_{\mathrm{c}}, \\ 0, & \text{if } r > r_{\mathrm{c}}, \end{cases} \quad (1)$$

where $r_c = 2.5\,\sigma$ is the cut-off distance and $u_0 = -0.0163\,\epsilon_{ij}$ is the shift of the potential at the cutoff. All particles are assumed to have the same mass m and size, the latter represented by a constant σ. ϵ_{ij} is the depth of the potential well for interactions between species i and j. We consider the case where $\epsilon_{11} = \epsilon_{22}$, and we will study different values of ϵ_{12}.

The evolution of the position $\boldsymbol{x}_i$ of particle i is described by the Langevin equation

$$m\ddot{\boldsymbol{x}}_i = -\boldsymbol{\nabla}_i U - \zeta \dot{\boldsymbol{x}}_i + \boldsymbol{\eta}_i(t), \quad (2)$$

where ζ is the particle's drag coefficient, $\boldsymbol{\nabla}_i U$ is the gradient of the global potential energy U with respect to $\boldsymbol{x}_i$, and $\boldsymbol{\eta}_i(t)$ is a Gaussian random force independent for all particles, with zero mean and with variance $\langle \boldsymbol{\eta}_i(t) \cdot \boldsymbol{\eta}_i(t') \rangle = 2k_{\mathrm{B}} T \zeta \delta(t' - t)$.

In the following, we use reduced Lennard-Jones units based on m, σ, ϵ_{11} and $\epsilon_{11}/k_{\mathrm{B}}$ as units of mass, length, energy and temperature, respectively. The relative fraction of species i in the mixture is $x_i = N_i/N$, where N_i is the number of particles, and $x_1 + x_2 = 1$. A two-dimensional, rectangular box with periodic boundary conditions and dimensions $L_y = \sqrt{3} L_x$ is used in order to be compatible with the triangular crystal phase of the monodisperse Lennard-Jones model. We define the simulation box size by the surface $S = L_x L_y$ (denoting a two-dimensional "volume"). The average isotropic pressure is kept constant at $P = 2$, since this value allows comparing to results from previous studies [30,31].

2.2 Simulation aspects

We perform molecular dynamics (MD) simulations using the LAMMPS code [32]. The temperature of each species is set using the Langevin thermostat provided by this computer program. The Langevin thermostat is controlled by its characteristic damping time $t_{\mathrm{damp}} = m/\zeta$, which is inversely proportional to the solvent viscosity. In our simulations we set $t_{\mathrm{damp}} = 0.01$ Lennard-Jones time units. Simulations run with different values of the t_{damp} parameter showed that such a low value is required so that the temperatures of the two species are kept within 2.5% of their desired values, whereas larger values of the t_{damp} parameter led to temperature uniformity between the two species. Because the required value of t_{damp} is small compared to the Lennard-Jones unit time, particle diffusion coefficients are also small, and this requires longer simulation times in order for the system to reach its steady

Table 1. Summary of the simulation parameters. Boldface values are kept constant throughout this study. Lightface values define our reference conditions but change for different cases. Values are expressed in Lennard-Jones units, with m, σ, ϵ_{11} and $\epsilon_{11}/k_{\mathrm{B}}$ as units of mass, length, energy and temperature, respectively.

Symbol	Meaning	Value
N	Number of particles	**1250**
x_1	Fraction of particles of type 1	0.5
ϵ_{12}	Potential interaction between 1 and 2	1
ϵ_{22}	Potential interaction of species 2	**1**
r_{cut}	Potential cut-off distance	**2.5**
P	Pressure	**2**
T^*	Average temperature of all particles	variable
ΔT	Temperature difference, $T_1 - T_2$	variable
t_{damp}	Langevin thermostat damping time	**0.01**
$\mathrm{d}t$	Simulation time step	$\mathbf{2.5 \cdot 10^{-3}}$

state. This state, also referred to as "equilibrium" state in the paper, does not imply thermal equilibrium (same temperature) between the two species. Indeed, if $\Delta T > 0$, a constant energy flux is added by the thermostat to the hot particles and removed from the cold particles (see Electronic Supplementary Material (ESM) for more details).

Table 1 summarizes the simulation parameters. Each simulation series is defined by a set of parameter values ΔT, x_1, ϵ_{12}. For each series, we study different cases by gradually increasing the average system temperature, $T^* = x_1 T_1 + x_2 T_2$, while fixing the pressure $P = 2$. The initial particle configuration for the first case in each series is a triangular array of particles with random initial velocities. The initial spots within the array of particles of types 1 and 2 are chosen at random to produce an initial configuration that respects the prescribed value of x_1. The temperature T^* of the initial case is sufficiently low so that the system is at a solid state. For the following cases in the series, each having a higher temperature than the previous one, the initial particle configuration is taken as the final configuration of the previous case. All simulations are performed with a MD integration time step $\mathrm{d}t = 0.0025$. Results for each T^* are obtained after four stages. Stage one consists in using the isoenthalpic-isobaric ensemble NPH with a Nose-Hoover barostat coupled with a Langevin thermostat (NPH-L). The system is heated at a rate $\mathrm{d}T/\mathrm{d}t = 10^{-5}$ until the desired temperature is reached. Then, as stage two, it is stabilized for an additional $7 \cdot 10^6$ time steps. The simulation is then continued using the micro-canonical ensemble NVE coupled with a Langevin thermostat (NVE-L), and with the volume fixed at the equilibrium value reached in the NPH-L simulation (stage 3). The system is let to equilibrate for $3 \cdot 10^6$ time steps. Finally, as stage 4, results are obtained by averaging the statistics over an additional $8 \cdot 10^6$ time steps. We verify that the pressure at this final stage fluctuates around a mean value of $P = 2$ and with a standard deviation of about 5%. The number of simulation steps was chosen by performing a convergence analysis of the thermomechanical characteristics of the mixture. In order to improve the accuracy of the results, each simulation series is repeated 8 independent times, each time using different initial velocities and different seeds for the random number generators. We report the average values and standard deviations over the 8 MD runs.

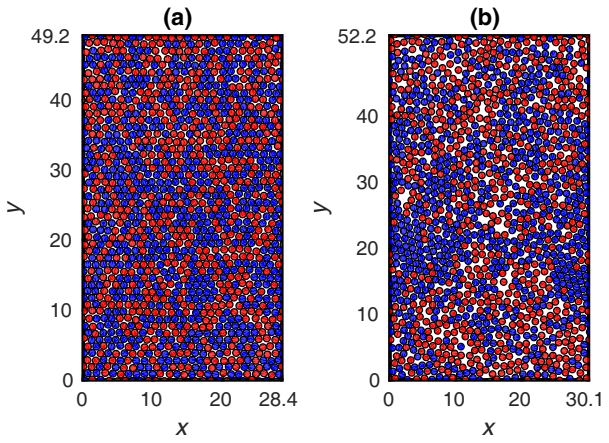

Fig. 1. Snapshots of the system at steady state for $x_1 = 0.5$, $\epsilon_{12} = 1$, $\Delta T = 0.6$, and (a) $T^* = 0.5$ ($T_1 = 0.8$, $T_2 = 0.2$) or (b) $T^* = 0.7$ ($T_1 = 1.0$, $T_2 = 0.5$). The hotter species (1) is represented in red and the colder species (2) in blue.

2.3 Computation of thermomechanical properties

We characterize the macroscopic mechanical behavior of our system by computing the shear modulus G and the bulk modulus K, whose macroscopic definitions are $G = \delta\tau/\delta\gamma_{xy}$, the ratio between the average shear stress and a small shear strain, and $K = \rho(\partial P/\partial\rho)_T$, with $\rho = N/S$ the particle density. These parameters have been used to experimentally characterize the mechanical response of active, living tissues [33]. To compute these properties, we impose six different types of deformation of the simulation box, in order to induce a strain $\epsilon_{xx} = \pm 0.01$ or $\epsilon_{yy} = \pm 0.01$ or $\epsilon_{xy} = \gamma_{xy}/2 = \pm 0.01$. After system equilibration, we evaluate the terms of the stress tensor and deduce the parameters G and K. The final values are obtained by averaging over 8 independent simulations. The value of the imposed strain was chosen from numerical tests that showed moduli results to become independent of the value of ϵ for $\epsilon \geq 0.01$.

3 Results and discussion

To illustrate the nature of our simulations, fig. 1 shows snapshots of "equilibrated" (steady-state) systems with $x_1 = 0.5$, $\epsilon_{12} = 1$, $\Delta T = 0.6$. Species 1, represented by red disks, are the hotter or *active* particles, and species 2, represented by blue disks, are the colder or *passive* particles.

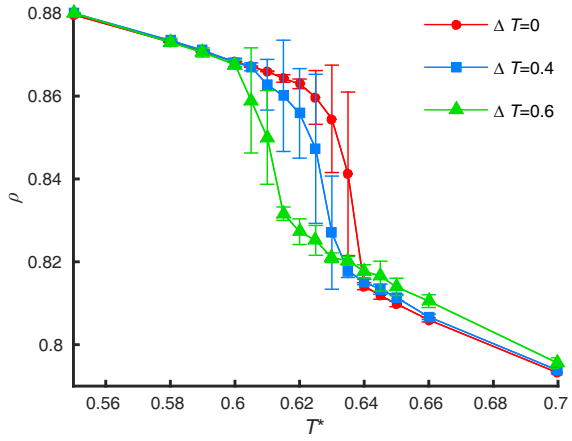

Fig. 2. Density ρ as a function of the average temperature T^* for $x_1 = 0.5$, $\epsilon_{12} = 1$, and $\Delta T = 0$ (red circles), 0.4 (blue squares), and 0.6 (green triangles). Error bars are standard deviations over 8 independent MD runs.

The two species are mixed without marked segregation. The hotter particles appear to be slightly more disordered than the colder particles, as will later be confirmed by comparison of their respective partial radial distribution functions. Plot (a) corresponds to $T^* = 0.5$, where the system is at the solid state and the particles are sensibly more ordered than in plot (b), corresponding to $T^* = 0.7$, above the solid-liquid phase transition temperature.

3.1 Shift of the liquid-solid phase transition due to colloidal activity

Figure 2 shows the evolution of density $\rho = N/S$ as a function of the average temperature T^* for different values of the temperature difference between the two species, ΔT. The solid-to-liquid phase transition is identified by the discontinuous density drop at the melting temperature. For a one-component Lennard-Jones system, or equivalently for a mixture of two identical species at the same temperature ($\Delta T = 0$), melting occurs at about $T_\mathrm{m} \approx 0.63$. As ΔT is increased, the transition temperature shifts to smaller and smaller values, with $T_\mathrm{m} \approx 0.61$ for $\Delta T = 0.6$. Moreover, the transition becomes more gradual, with less steep and smaller density drop. This striking result indicates that, near the melting temperature, a mixture of active and passive colloids can behave as a liquid, whereas a one-component system at the same average temperature behaves as a solid. This key result of our work is not specific to our characterization of the system by its average temperature T^*. A similar conclusion is reached if an "equivalent temperature" in the liquid phase is defined based on mean-square particle displacements (see ESM). From fig. 2, one can also observe that for T^* in the liquid range, at a given T^*, the density of the liquid increases (slightly) with ΔT. This shows a distinct effect of the colder species.

To characterize the state of the binary mixture at different temperatures, we investigated the mean square displacement (MSD) and the radial distribution functions (RDFs) of the two particle populations. Figure 3 shows the results for a mixture with $\Delta T = 0.6$ and either $T^* = 0.55$ (left) or $T^* = 0.65$ (right). As the phase transition temperature is around 0.61, these two cases correspond respectively to a solid and a liquid close to the transition. For the solid at $T^* = 0.55$, the MSD (fig. 3(a)) is very small and does not significantly evolve over time. Agitation of the hot particles is slightly larger than that of the cold particles. The RDF (fig. 3(c)) indicates a hot crystal, with peaks corresponding to the coordination layers in a crystalline triangular lattice. We represent the total RDF g_all as well as g_{11} (hot particles), g_{22} (cold particles), and g_{12}. All four functions display features of a hot crystal. These functions are quite close to one another, with nevertheless the cold particles exhibiting a more ordered structure than the hot particles. We have also compared g_all with the radial distribution function of a one-component system at $T = T^* = 0.55$ and found that both functions are virtually identical (see inset). The MSD at $T^* = 0.65$ (fig. 3(b)) increases linearly over time, as characteristic of diffusion in a liquid. The overall MSD is virtually identical to that of a one-component system at $T = T^* = 0.65$. When we consider the two species separately, we observe that the MSD of the hot particles ($T_1 = 0.95$, red solid line) is larger than the overall MSD (black solid line), which in turn is larger than the MSD of the cold particles ($T_2 = 0.35$, blue solid line). We have also compared the MSD for each species in the mixture with that of a one-component system at the species temperature. Thus, we recall that the solid red line corresponds to the hot species ($T_1 = 0.95$) in the binary mixture. This is to be compared to the dotted red line, corresponding to a one-component system at $T = 0.95$ and the same pressure as the mixture ($P = 2$). We also consider a one-component system at $T = 0.95$ at a volume fixed at that of the mixture, which is smaller than that of the hot species alone. By comparing the three curves, we conclude that the MSD of the hot species is reduced when they are in the mixture, partly because of the smaller volume of the mixture (dotted red line to dashed red line), and partly because of interactions with the cold species (dashed red line to solid red line). A similar discussion is valid for the cold species. Although in this case the volume effect is negligible, interactions with the hot species clearly lift the slope of the MSD of the cold particles in the mixture, from solid-like to liquid-like. The RDFs for $T^* = 0.65$ are shown in fig. 3(d). At short distances, they show some structure, more than in a typical hot simple liquid [34]. As they all oscillate around 1 at long distances, the system is certainly in a disordered state. Combined with the MSD information of fig. 3(b), these RDFs represent indeed a liquid state. We notice a significant difference between g_{11} and g_{22}, indicating that the cold particles retain more order. Overall, this analysis shows that the binary system of active and passive particles has an average behavior corresponding to that of a one-component system at the average temperature. However, the behaviors of active and passive particles differ when the two species are considered separately.

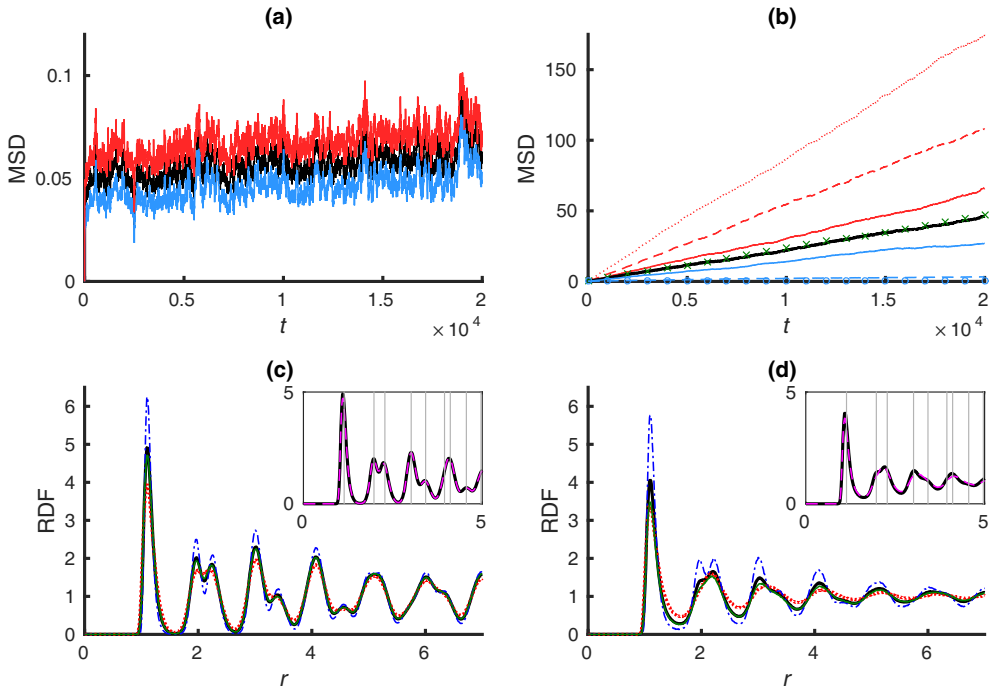

Fig. 3. Characterization of binary mixtures with $x_1 = 0.5$ and $\epsilon_{12} = 1$. (a) Mean square displacement (MSD) for a mixture with $T^* = 0.55$ and $\Delta T = 0.6$ for all particles (black line), for the hot particles at $T_1 = 0.85$ (red line, lighter), and for the cold particles at $T_2 = 0.25$ (blue line, lightest). (b) MSD for a mixture with $T^* = 0.65$ and $\Delta T = 0.6$ for all particles (solid black line), for the hot particles at $T_1 = 0.95$ (solid red line, lighter), and for the cold particles at $T_2 = 0.35$ (solid blue line, lightest). The results are compared to a one-component system at $T = 0.65$ and the same density as the mixture (green crosses), to a one-component system at $T = 0.95$ and having either the mixture's density (dashed red line) or the density corresponding to $P = 2$ (dotted red line), and to a one-component system at $T = 0.35$ and either the mixture's density (dashed blue line) or the density corresponding to $P = 2$ (blue circles, superimposed to the horizontal axis). (c) Radial distribution function (RDF) for a mixture with $T^* = 0.55$ and $\Delta T = 0.6$ for all particles (thick solid black line) and partial RDFs g_{11} (dotted red line), g_{22} (dash-dotted blue line), g_{12} (thin solid green line). The inset compares the total RDF of the mixture (solid black line) with the RDF of a one-component system at $T = 0.55$ and the same density as the mixture (dashed magenta line). The vertical gray lines indicate the theoretical peak positions in a perfect crystal. (d) RDFs for a mixture with $T^* = 0.65$ and $\Delta T = 0.6$. The color code is the same as in plot c.

3.2 Modulation of thermomechanical properties by colloidal activity

Next we investigate the thermomechanical properties of the binary mixture. Figure 4 shows the evolution of the shear modulus, G, and the bulk modulus, K, as a function of the average temperature, T^*, for different values of the temperature difference between the two species, ΔT. The results are consistent with the shift in phase transition with increasing ΔT, shown in fig. 2 above. The study of the elastic moduli confirms that the phase transition is shifted to smaller temperatures with increasing ΔT. Moreover, we observe that, for a given average temperature T^* in the vicinity of the phase transition, the elastic moduli become smaller with increasing ΔT. We thus conclude that increasing the effective temperature difference between the active and passive components fluidifies the system (because the melting temperature decreases) and renders it more deformable (because the elastic moduli decrease). Quantitatively, we observe that both G and K show strong signatures of the melting transition. Furthermore, they indicate the same transition temperature as the density criterion (cf. fig. 2). This shows the consistency of our results. We also verify that, as expected, the shear modulus in the liquid vanishes for all ΔT. We have also investigated the possibility of computing thermomechanical properties using the stress fluctuation formalism [35, 36] based on the average temperature of the system. This alternative approach is efficient and exact for $\Delta T = 0$, whereas it provides an approximate result for $\Delta T > 0$ (see discussion and fig. S2 in the ESM).

3.3 Effects of mixture composition and of interspecies interaction

Previous results correspond to an equimolar mixture ($x_1 = x_2 = 0.5$) with uniform particle interactions ($\epsilon_{11} = \epsilon_{22} = \epsilon_{12} = 1$). In this section we investigate the effects of changing the composition (x_1) or the interspecies interaction (ϵ_{12}).

Figure 5 shows the effect of changing x_1 on the phase transition, identified by the rapid changes in ρ and in G as a function of the average temperature T^*. Here,

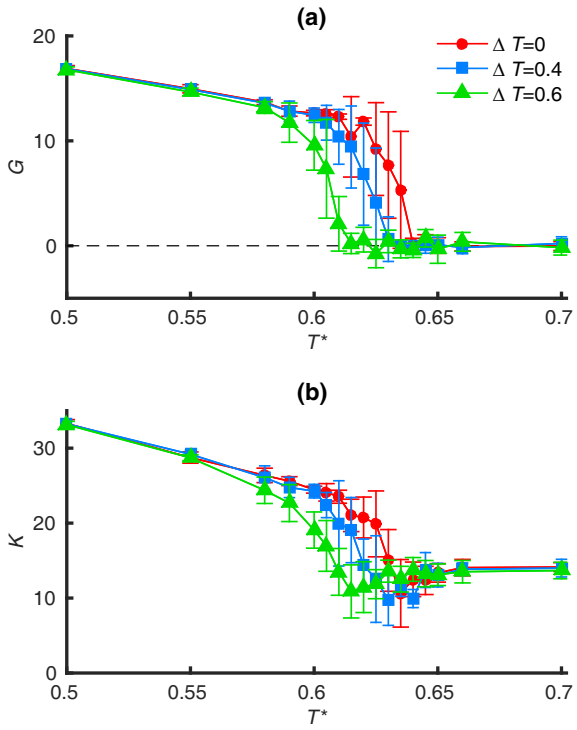

Fig. 4. Characterization of thermomechanical properties of binary mixtures with $x_1 = 0.5$ and $\epsilon_{12} = 1$. (a) Shear modulus G and (b) bulk modulus K as a function of the average temperature T^* for $\Delta T = 0$ (red circles), $\Delta T = 0.4$ (blue squares), and $\Delta T = 0.6$ (green triangles). Error bars are standard deviations over 8 independent MD runs.

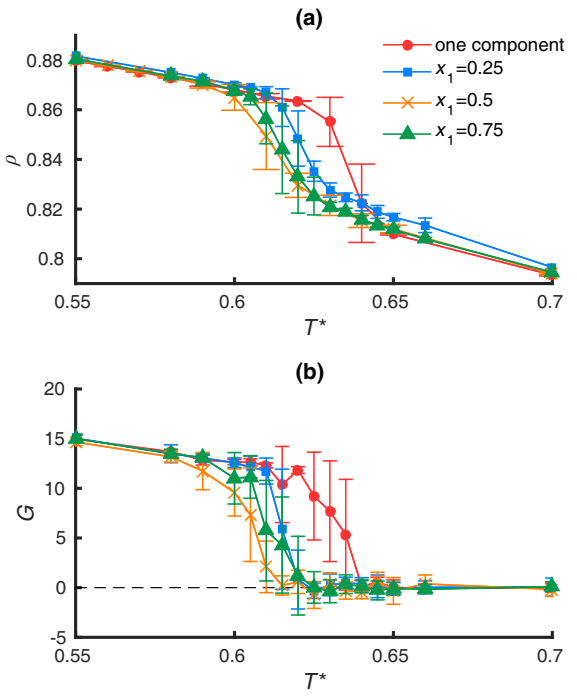

Fig. 5. Phase-transition characterization of a binary mixture with $\epsilon_{12} = 1$ and different fractions of the hot species, x_1. (a) Density ρ and (b) shear modulus G as a function of average temperature T^* for a one-component system (red circles) and mixtures with $\Delta T = 0.6$ and $x_1 = 0.25$ (blue squares), $x_1 = 0.50$ (orange crosses), or $x_1 = 0.75$ (green triangles). Error bars are standard deviations over 8 independent MD runs.

a mixture with $\Delta T = 0.6$ is studied. We recall that increasing ΔT shifts the transition to a lower melting temperature. This effect is maximum for an equimolar mixture ($x_1 = 0.5$), and it is attenuated when one of the two species is dominant. Indeed, when $x_1 = 0$ or $x_1 = 1$ we retrieve a one-component system, and the result is the same as for the one-component system considered in figs. 2 and 4 ($x_1 = 0.5$ and $\Delta T = 0$). The corresponding results obtained by application of the stress fluctuation formalism based on the average temperature are presented in fig. S3 of the ESM.

Figure 6 illustrates the effect of varying the interparticle energy parameter ϵ_{12}, which we refer to as the "interparticle affinity" parameter. The corresponding results obtained by application of the stress fluctuation formalism based on the average temperature are presented in fig. S4 of the ESM. Three particle affinities are considered: a heterocoordinated system with $\epsilon_{12} = 1.5$ (red curves), the reference case with $\epsilon_{12} = 1$ (blue curves), and a homocoordinated system with $\epsilon_{12} = 0.5$ (green curves). Varying ϵ_{12} has a marked effect on the melting temperature, as seen in the figure. Here we focus on the interplay between the effects of interparticle affinity and of the difference in effective temperatures. Thus, for each of the three values of ϵ_{12}, we compare a mixture where all particles have the same effective temperature ($\Delta T = 0$) with a mixture where the two components have different effective temperatures ($\Delta T = 0.6$). As discussed above, increasing ΔT shifts the transition to a lower temperature. As shown in the figure, this effect is more pronounced in a homocoordinated system, where each particle type (active or passive) interacts more strongly with its own kind.

Figure 7(a) and (b) show the RDF for two binary mixtures at the liquid state to illustrate heterocoordination ($\epsilon_{12} = 1.5$) and homocoordination ($\epsilon_{12} = 0.5$). In a heterocoordinated system (fig. 7(a)) we observe that the first peak of g_{12} (green solid line) is significantly more pronounced than the global RDF for all particles, g_{all} (black solid line). The opposite is observed at a homocoordinated system (fig. 7(b)).

As we can expect, when ϵ_{12} is so small compared to $(\epsilon_{11} + \epsilon_{22})/2 = \epsilon_{11}$, the system could demix, especially in low-temperature liquid phase. This possibility exists even when $\Delta T = 0$, as a simple demixing theory would indicate [37]. Increasing ΔT will certainly favor this segregation. Figure 7(c) and (d) show snapshots of a liquid binary mixture ($T^* = 0.8$) with $\epsilon_{12} = 0.5$ and either $\Delta T = 0$ (plot (c)) or $\Delta T = 0.6$ (plot (d)). In the absence of effective temperature difference, reduced interparticle affinity ($\epsilon_{12} = 0.5$) favors homocoordonation, but the two particle types remain mixed (plot (c)). In contrast, the joint effect of reduced interparticle affinity and effective temperature difference leads to segregation between the two components (plot (d)). This segregation is also signaled by the

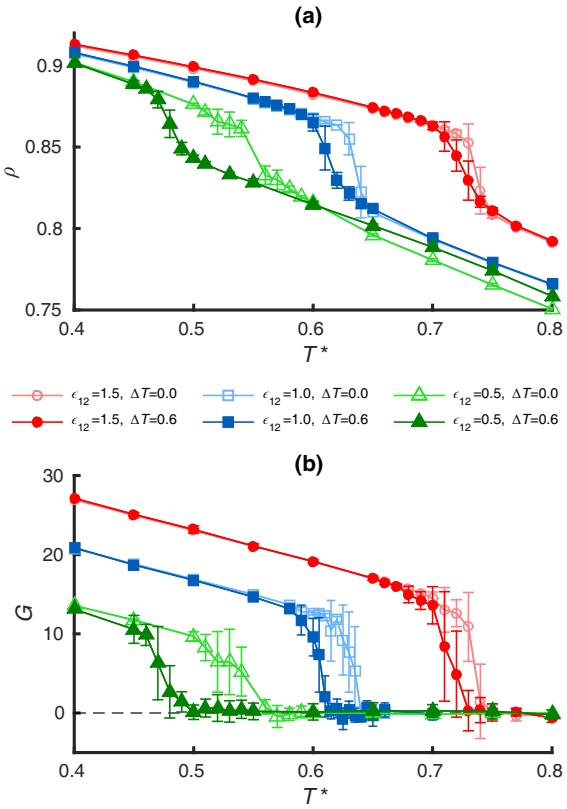

Fig. 6. Phase-transition characterization of a binary mixture with $x_1 = 0.5$ and different interparticle affinities ϵ_{12}. (a) Density ρ and (b) shear modulus G as a function of average temperature T^* for a mixture with either $\Delta T = 0$ (lighter empty markers) or $\Delta T = 0.6$ (darker full markers) for three different interparticle interactions: $\epsilon_{12} = 1.5$ (red circles), $\epsilon_{12} = 1.0$ (blue squares), or $\epsilon_{12} = 0.5$ (green triangles). Error bars are standard deviations over 8 independent MD runs.

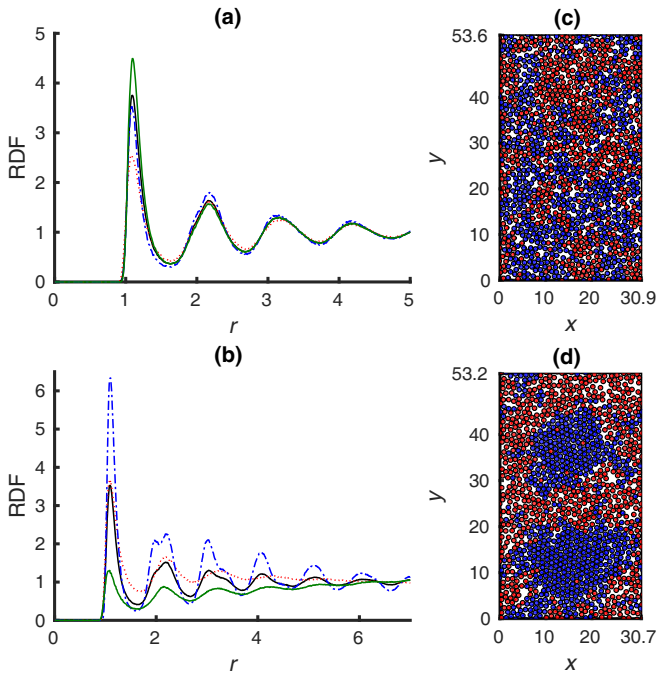

Fig. 7. Structure of binary mixtures with $x_1 = 0.5$ and different interparticle affinities. (a) A mixture with $T^* = 0.8$, $\Delta T = 0.6$, and $\epsilon_{12} = 1.5$. Radial distribution function for all particles (thick solid black line) and partial radial distribution functions g_{11} (dotted red line), g_{22} (dash-dotted blue line), g_{12} (thin solid green line). (b) A mixture with $\epsilon_{12} = 0.5$. All other parameters as well as the color code are identical to plot a. (c) Snapshot at steady state for a mixture of two species at the same temperature, $T_1 = T_2 = T^* = 0.8$ ($\Delta T = 0$) and $\epsilon_{12} = 0.5$. (d) Snapshot at steady state for a mixture with $T^* = 0.8$, $\Delta T = 0.6$, and $\epsilon_{12} = 0.5$. The hotter species is represented in red and the colder in blue.

g_{12} function in fig. 7(b), with conspicuously little structure. It is noted that segregation between the two components can also be obtained with neutral interparticle affinity ($\epsilon_{12} = 1$) if the effective temperature difference is sufficiently large. Indeed, we have observed segregation in simulations run with $\epsilon_{12} = 1$ and $\Delta T = 0.8$ for certain liquid state temperatures T^*. This finding is consistent with the conclusions of [7], where it was argued that in case of comparable interaction features, a large difference in the kinetic energies of the two species would lead to a segregated steady state (in the liquid phase). To summarize, we observe that the segregation depends on three key parameters, ϵ_{12}, ΔT, and T^* (very hot liquids tend to mix well).

4 Conclusion

We have investigated the behavior of a two-dimensional mixture of active and passive colloids with Lennard-Jones interactions. Active colloids are characterized by an effective temperature that is higher than that of passive colloids. We have investigated the solid-to-liquid phase transition of the system. We found that the average temperature at melting of a mixture of active and passive colloids is lower than that of a one-component system. Inclusion of an active component obviously makes the system "hotter" on average and favors transition to the liquid state. Strikingly, our findings show that this effect is more pronounced than expected from the linear average temperature of the system. This "enhanced softening" of the mixture increases with differential activity, *i.e.*, the difference in effective temperature between the two components. Our calculations of thermomechanical properties show that, at any given average temperature of the system in the vicinity of the melting transition, an increase of differential activity between the two components reduces the melting temperature as well as the shear and compressibility moduli. This "enhanced softening" effect constitutes the central result of our paper.

As discussed in the introduction, a perspective of studying hybrid aggregates is to develop cancer therapies based on particles. Doping a tumor with passive particles could rigidify it and limit its spreading. When projected to this biomedical application, our results warn us that the effect of passive particle doping may be less than anticipated by an argument based on linearly averaging the properties of the two components.

Consistent with earlier findings [7,20,21], segregation between the active and passive components may occur due to differential activity, differential particle affinity, or a combination of both. Differential activity may induce segregation on its own, but in our simulations this only occurs when the effective temperature of the active colloids is much larger than the temperature of passive colloids. This result is encouraging to the perspective of doping a tumor with passive colloids, as homogeneous mixing can be obtained. This conclusion is supported by the experimental realization of well-mixed hybrid cell-particle aggregates [16]. When drawing such biological implications, we acknowledge that the model studied here remains very idealized, and it lacks many of the features of the real biophysical systems. We aim to reduce this gap in our future work.

This work has been partially funded by the European Union through the program *FEDER-FSE Lorraine et Massif des Vosges 2014-2020*. The PMMS (Pôle Messin de Modélisation et de Simulation) is gratefully acknowledged for providing us with computer time.

Author contribution statement

HX and DGR designed and directed the study. ME and SH performed the computations. All the authors analyzed and discussed the results. HX and DGR wrote the paper with input from all the authors.

References

1. D. Marenduzzo, Eur. Phys. J. ST **225**, 2065 (2016).
2. A.P. Solon, M.E. Cates, J. Tailleur, Eur. Phys. J. ST **224**, 1231 (2015).
3. C. Touya, T. Schwalger, B. Lindner, Phys. Rev. E **83**, 051913 (2011).
4. F. Ginot, A. Solon, Y. Kafri, C. Ybert, J.T.T. Cottin-Bizonne, New J. Phys. **20**, 115001 (2018).
5. P. Melby, F.V. Reyes, A. Prevost, R. Robertson, P. Kumar, D.A. Egolf, J.S. Urbach, J. Phys. Condens. Matter **17**, S2689 (2005).
6. A. Agrawal, N. Ganai, S. Sengupta, G.I. Menon, J. Stat. Mech. **26**, 014001 (2017).
7. A.Y. Grosberg, J.F. Joanny, Phys. Rev. E **92**, 032118 (2015).
8. M. Schienbein, K. Franke, H. Gruler, Phys. Rev. E **49**, 5462 (1994).
9. J.C.M. Mombach, J.A. Glazier, Phys. Rev. Lett. **76**, 3032 (1996).
10. D. Drasdo, S. Höhme, Phys. Biol. **2**, 133 (2005).
11. J. Ranft, M. Basan, J. Elgeti, J.F. Joanny, J. Prost, F. Jülicher, Proc. Natl. Acad. Sci. U.S.A. **107**, 20863 (2010).
12. M. Basan, J. Prost, J.F. Joanny, J. Elgeti, Phys. Biol. **8**, 026014 (2011).
13. P. Van Liedekerke, J. Neitsch, T. Johann, K. Alessandri, P. Nassoy, D. Drasdo, PLoS Comput. Biol. **15**, e1006273 (2019).
14. D. Gonzalez-Rodriguez, K. Guevorkian, S. Douezan, F. Brochard-Wyart, Science **338**, 910 (2012).
15. D.L. Hu, S. Phonekeo, E. Altshuler, F. Brochard-Wyart, Eur. Phys. J. ST **225**, 629 (2016).
16. B. Brunel, G. Beaune, U. Nagarajan, S. Dufour, F. Brochard-Wyart, F.M. Winnik, Soft Matter **12**, 7902 (2016).
17. G. Beaune, U. Nagarajan, F. Brochard-Wyart, F.M. Winnik, Langmuir **35**, 7396 (2019).
18. M. Han, J. Yan, S. Granick, E. Luijten, Proc. Natl. Acad. Sci. U.S.A. **114**, 7513 (2017).
19. Y. Fily, M.C. Marchetti, Phys. Rev. Lett. **108**, 235702 (2012).
20. S.N. Weber, C.A. Weber, E. Frey, Phys. Rev. Lett. **116**, 058301 (2016).
21. H. Tanaka, A.A. Lee, M.P. Brenner, Phys. Rev. Fluids **2**, 043103 (2017).
22. J. Bialké, T. Speck, H. Löwen, Phys. Rev. Lett. **108**, 168301 (2012).
23. G. Briand, O. Dauchot, Phys. Rev. Lett. **117**, 098004 (2016).
24. P. Digregorio, D. Levis, D.L. Suma, L.F. Cugliandolo, G. Gonnella, I. Pagonabarraga, Phys. Rev. Lett. **121**, 098003 (2018).
25. R. Ni, M.A. Cohen Stuart, M. Dijkstra, Nat. Commun. **4**, 2704 (2013).
26. R. Ni, M.A. Cohen Stuart, M. Dijkstra, P.G. Bolhuis, Soft Matter **10**, 6609 (2014).
27. S.R. McCandlish, A. Baskaran, M.F. Hagan, Soft **8**, 2527 (2012).
28. J. Stenhammar, R. Wittkowski, D. Marenduzzo, M.E. Cates, Phys. Rev. Lett. **114**, 018301 (2015).
29. T.F.F. Farage, P. Krinninger, J.M. Brader, Phys. Rev. E **91**, 042310 (2015).
30. J.P. Wittmer, H. Xu, P. Polinska, F. Weysser, J. Baschnagel, J. Chem. Phys. **138**, 12A533 (2013).
31. D. Li, H. Xu, J.P. Wittmer, J. Phys.: Condens. Matter **28**, 045101 (2016).
32. S. Plimpton, J. Comput. Phys. **117**, 1 (1995).
33. M. Delarue, J.F. Joanny, F. Jülicher, J. Prost, Interface Focus **4**, 20140033 (2014).
34. J.P. Hansen, I.R. McDonald, *Theory of Simple Liquids*, 2nd edition (Academic Press, 1986).
35. D.R. Squire, A.C. Holt, W.G. Hoover, Physica **42**, 388 (1969).
36. D. Li, H. Xu, Mol. Phys. **115**, 3104 (2017).
37. R.H. Colby, M. Rubinstein, *Polymer Physics* (Oxford University Press, New York, 2003).